Chinese Chemical Letters 34 (2023) 108307

Contents lists available at ScienceDirect

Chinese Chemical Letters

journal homepage: www.elsevier.com/locate/cclet

Research progress of "rocking chair" type zinc-ion batteries with zinc metal-free anodes

Le Li[a], Shaofeng Jia[a], Minghui Cao[c], Yongqiang Ji[e], Hengwei Qiu[d,*], Dan Zhang[b,*]

[a] Shaanxi Key Laboratory of Industrial Automation, School of Mechanical Engineering, Shaanxi University of Technology, Hanzhong 723001, China
[b] Shaanxi Key Laboratory of Catalysis, School of Chemistry and Environment Science, Shaanxi University of Technology, Hanzhong 723001, China
[c] School of Electronic and Information Engineering, Qingdao University, Qingdao 266071, China
[d] Department of Chemistry, Key Laboratory of Bioorganic Phosphorus Chemistry and Chemical Biology, Tsinghua University, Beijing 100084, China
[e] State Key Laboratory for Artifcial Microstructure and Mesoscopic Physics, School of Physics, Peking University, Beijing 100871, China

ARTICLE INFO

Article history:
Received 10 January 2023
Revised 3 February 2023
Accepted 6 March 2023
Available online 11 March 2023

Keywords:
Zinc ion batteries (ZIBs)
"Rocking chair" type
Zinc metal-free anode
Transition metal dichalcogenides
Transition metal oxides
Organic compounds

ABSTRACT

"Rocking chair" type lithium-ion batteries with lithium metal-free anodes have been successfully commercialized over the past few decades. Zinc-ion batteries (ZIBs) have gained increasing attention in recent years given their safety, greenness, ease of manufacture, and cost-efficiency. Nevertheless, the practical application of ZIBs is largely hindered by the dendritic growth of the Zn metal anode, low Coulombic efficiency, great harm, and existence of various side reactions. Herein, this review provides a systematic overview of emerging "rocking chair" type ZIBs with zinc metal-free anodes. Firstly, the basic fundamentals, advantages, and challenges of "rocking chair" type ZIBs are introduced. Subsequently, an overview of the design principles and recent progress of "rocking chair" type ZIBs with zinc metal-free anodes are presented. Finally, the key challenges and perspectives for future advancement of "rocking chair" type ZIBs with zinc metal-free anodes are proposed. This review is anticipated to attracted increased focus to metal-free anodes "rocking chair" type metal-ion battery and provide new inspirations for the development of high-energy metal-ion batteries.

1. Introduction

As the world becomes increasingly aware of the effects of climate change, numerous nations have established objectives to raise the proportion of renewable energy in their overall energy production [1]. Consequently, the need for cost-effective and secure energy storage technologies to store electrical energy generated from renewable sources and then feed it into the grid has become an imperative for our society [2,3]. Lithium-ion batteries (LIBs) are one of the go-to energy storage devices with high efficiency, long life, high energy density, and low maintenance cost; they have dominated the market for decades [4–7]. However, the dearth of Li on Earth, the use of flammability and toxicity of organic electrolytes, and other safety concerns seriously limit the widespread usage of Li [8,9]. As an alternative, research on batteries based on multivalent charge carriers, such as Zn^{2+}, Mg^{2+}, Ca^{2+} and Al^{3+}, have received extensive attention. Zinc-ion batteries (ZIBs) deliver greater potential for extensive energy storage applications than LIBs and other electrochemical energy storage devices: (1) High theoretical capacity (820 mAh/g, 5851 mAh/cm^3) and low electrochemical potential (−0.763 V *vs.* the standard hydrogen electrode) of Zn metal (Fig. 1) [10,11]; (2) High ionic conductivity of aqueous electrolytes is attributed to compatible cation and hydrated radius of Zn^{2+} [12,13]; (3) High energy density of Zn anode due to two-electron transfer during redox reactions; (4) Excellent ambient environment stability, cost-effective (2 USD/kg) and non-toxic of Zn; (5) Effortless processing of material and production of battery [14,15].

Despite these advantages of ZIBs, various drawbacks such as corrosion, dendrite growth, hydrogen evolution reaction (HER), and by-products still exist, hindering the large-scale application of ZIBs [16–25]. Reports have been that during Zn^{2+} electroplating, Zn dendrites always originate from uneven Zn deposition, which is practically unavoidable due to the microenvironment at the electrolyte and anode interface (*e.g.*, anode flatness and anode surface electric field distribution) and the distribution of Zn^{2+} in the electrolyte cannot be maintained uniform and constant, resulting in a tip effect [26–28]. The formation of uncontrolled Zn dendrites has a direct impact on the Coulombic efficiency (CE) and cycle life of ZIBs, and can even lead to a short circuit by piercing the sep-

* Corresponding authors.
E-mail addresses: qiuhengwei@mail.tsinghua.edu.cn (H. Qiu), zhangdan@snut.edu.cn (D. Zhang).

https://doi.org/10.1016/j.cclet.2023.108307
1001-8417/

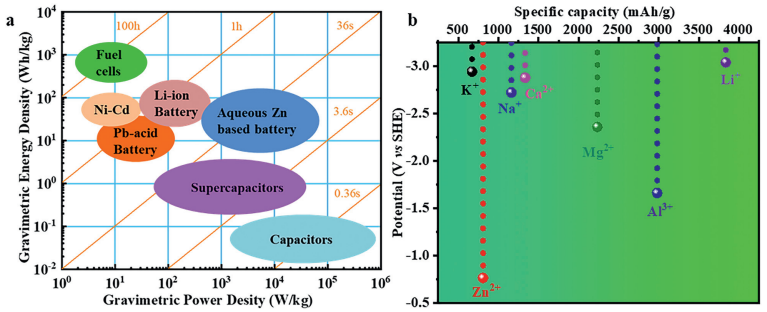

Fig. 1. (a) Ragone plot of some electrochemical energy storage devices, (b) Comparison of potential and specific capacitance of metal-ion (Li^+, Na^+, K^+, Zn^{2+}, Mg^{2+}, Al^{3+}) batteries.

arator and bridging the positive electrode [29,30]. Generally, the two types of water molecules in water electrolytes are free water molecules and solvated water molecules [31–33], and the ratio of Zn^{2+} to water is 1:56 in the commonly employed $ZnSO_4$ electrolyte (2 mol/L). Additionally, during electrodeposition, Zn^{2+} ions have a tendency to form tight ion pairs ($[Zn(H_2O)_6]^{2+}$) composed of six free water molecules [34]. As a result, a large number of active water molecules exist at the electrolyte and anode interface, exhibiting diversified side effects. In general, the active H_2O molecules generated after solvation of Zn^{2+} are easily broken down into OH^- and H^+ [35,36], and the accumulated H^+ ions are easily reduced to H_2 by gaining electrons from Zn, and then they escape from the electrolyte, leading to severe anode corrosion and HER effect [37]. Furthermore, in the entire pH range, the equilibrium potential of H_2O/H_2 is higher than that of Zn^{2+}/Zn, thus leading to spontaneous hydrogen evolution and corrosion on the anode surface [38,39]. Subsequently, the increase in electrolyte pH and residuary OH^- ions exacerbates the generation of by-products ($Zn_4SO_4(OH)_6{\cdot}xH_2O$), which hinder ion/electron diffusion and negatively affect the reversibility of Zn, and this strongly bound zincate complex further promotes the formation of zinc dendrites [35,40]. Additionally, the increase in the ionic size of hydrated Zn^{2+} (5.5 Å) vastly increases the energy expenditure of Zn^{2+}-H_2O bond breaking during Zn^{2+} intercalation [41,42]. Thus far, many strategies to mitigate or suppress side reactions and Zn dendrites have been presented, including designing a protective layer on the Zn anode surface [43,44], regulating the crystallographic orientation of Zn deposition [45,46], modifying the current collector [47,48], optimizing the internal structure of the Zn anode [49,50], modifying the separators [51,52], alloying zinc anodes with other chemically inert metals [53,54], optimizing the electrolytes [55,56], and developing "rocking chair" type ZIBs with zinc metal-free anodes [57,58]. Among these strategies, "rocking chair" type ZIBs with zinc metal-free anodes have attracted remarkable attention due to its convenient preparation and cost-effectiveness. However, studies on this area are few, and relevant reviews are limited.

The present study provides a systematic overview of emerging "rocking chair" type ZIBs with zinc metal-free anodes. Initially, the basic fundamentals, advantages, and challenges of "rocking chair" type ZIBs are introduced. Next, an overview of the design principles and recent progress of "rocking chair" type ZIBs with zinc metal-free anodes are presented. Finally, the key challenges and perspectives for future advancement of "rocking chair" type ZIBs with zinc metal-free anodes are proposed.

2. Introduction to "rocking chair" type ZIBs with zinc metal-free anodes

The concept of rocking chair was initially suggested by Armand in the 1970s [59]. The rocking chair battery is based on metal ions (such as Li^+, Na^+, K^+ and Zn^{2+}) or metal ions and hydrogen ions can reversibly sway between the positive and negative electrodes. Thus, the idea of constructing a rechargeable energy storage system is mainly based on Li metallic-free anodes. In 1976, in the early stage of Li battery development, Besenhard and Eichinger first used Li intercalation graphite (LiC_6) as the anode of rocking chair LIB instead of metal Li [60]. The lithiation voltage of graphite, which is approximately 0.1 V in contrast to Li^+/Li, surpasses the deposition voltage of Li. The graphite anode can prevent the generation of detrimental Li dendrites [61]. Intercalation of the anode material (such as graphite) to replace the metallic lithium anode significantly improves the safety of the battery and promotes the evolution from metal Li batteries to rocking chair LIBs. This successful turn provides a reference for the future development and direction of rocking-chair ZIBs [62]. Similarly, an appropriate zinc metal-free anode with a higher working potential than metallic Zn can effectually prevent the formation of Zn dendrites and side reactions, thereby improving battery safety and cycle life, which may offer a viable option for ZIBs.

2.1. Working mechanism of "rocking-chair" type ZIBs

ZIBs of the "rocking chair" type exhibit a comparable structure and mechanism to "rocking chair" LIBs and are generally defined as ZIBs, where Zn is the host instead of Zn metal. "Rocking chair" type ZIBs consists of intercalated zinc metal-free anode, anode current collector, electrolyte, separator, cathode current collector, and Zn-rich cathode. The working mechanism of the zinc metal-free "rocking chair" type ZIB is also based on the reversible shuttle of divalent zinc between the zinc substrates through the electrolyte (Fig. 2) [63]. During charging, the divalent Zn^{2+} extracted from the cathode side diffuses through the electrolyte-soaked separator, and then the anode is inserted. During discharge, divalent Zn^{2+} is reversely inserted from the anode to the cathode through the electrolyte-impregnated separator.

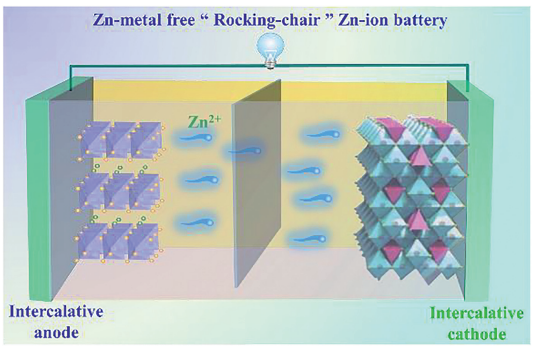

Fig. 2. Schematic illustration of the working principle of "rocking-chair" ZIBs.

2.2. Basic requirements of materials for "rocking-chair" type ZIBs

The "rocking chair" type ZIBs overcomes the safety problem of the metal Zn anode and have the advantages of long service life and low cost [64,65]. Zinc metal-free anodes are key components that affect battery performance and energy density and should satisfy the following criteria:

(1) Low Zn intercalation voltages. The weight/volume energy density of a battery depends on the operating voltage and the weight/volume specific capacity. Especially, the energy density is calculated by integrating voltage, current and discharge/charge time. The voltage of the battery is determined by the difference in potential between the positive and negative [64,66]. The large voltage gap between the positive and negative electrodes is crucial for improving the energy density of the full cell. In addition, longer and flat voltage plateaus are advantageous because they facilitate stable voltage output [64,61].
(2) High theoretical capacity. The energy density of a battery is determined by the specific capacity and operating voltage of the electrodes [67]. High capacity anodes are desirable. On the basis of previous literature [68], after determining the Zn^{2+} intercalation mechanism, the theoretical specific capacity of a given electrode material can be calculated in advance by the following formula:

$$\text{Theoretical specific capacity (mAh/g)} = nF/M \quad (1)$$

where n stands for the number of charge transfer, F is the Faraday constant (96485 C/mol), and M refers to molar weight (unit: g/mol).
(3) Low Zn^{2+} diffusion barriers. Zn^{2+} possesses a large hydrated ionic radius (4.04–4.30 Å), which leads to large steric hindrance and strong electrostatic interaction with the matrix [69], resulting in kinetic retardation and reduced Zn^{2+} intercalation and deintercalation rates. Therefore, the zinc metal-free should have a large interlayer distance or an appropriate tunnel structure to ensure the reversible and rapid intercalation and deintercalation of Zn^{2+} in the matrix [69].
(4) Stable structure. The reversible intercalation and deintercalation of Zn^{2+} generates large internal stress and destroys the structure. For high-performance zinc metal-free anodes, it is essential that they possess good structural stability to endure the process of Zn^{2+} insertion and deintercalation repeatedly. The alteration of the crystal structure causes ion channels to become defunct, resulting in increased diffusion resistance. Meanwhile, anode materials must have chemically and electrochemically stable electrode/electrolyte interfaces in the electrolyte to achieve stable cycling performance [70].
(5) High electronic conductivity. Poor electron conductivity hinders the migration and exchange of electrons. In addition, the low electronic conductivity leads to charge accumulation and strong electrostatic interaction between the anode host and Zn^{2+}, which slows down the diffusion rate of Zn ions.

2.3. Challenges of "rocking chair" type ZIB

The primary challenges of "rocking-chair" type ZIBs stem from the absence of high-performance host materials and the limited understanding of the Zn storage mechanism. The specific challenges are as follows:

(1) To date, very a small number of anodes have been investigated in "rocking chair" ZIBs. Rocking chair ZIB anodes have lower capacity than metallic zinc anodes. One of the greatest challenges facing burgeoning Zn-free rocking-chair ZIBs is their low energy density. In addition, the storage mechanism of zinc remains to be further studied. Rocking-chair ZIBs with high specific capacity, wide operating voltage, and long cycling stability should become the main direction of development.
(2) Studies on rocking chair ZIBs are few. Electrolytes suitable for rocking chair ZIBs ought to possess wide potential window, high ionic conductivity, and good electrolyte and electrode interface.
(3) The preparation technology of ZIBs is different from that of Zn metal batteries and non-aqueous LIBs. Especially, the electrode assembly technology and the selection of binders, current collectors, and containers remain a difficult task.

Therefore, considering the high research value and challenges of zinc metal-free "rocking-chair" ZIBs, a systematic summary is provided to offer insight into potential future exploration directions and the selection of high-performance electrode materials.

3. Zn-metal free anodes for "rocking chair" type ZIBs

Similar to Li and Na metal anodes, Zn metal anodes are susceptible to low CE and dendrite growth during galvanizing/stripping in both aqueous and non-aqueous systems [64,65]. Ideally, anode-free designs could enhance the whole energy performance of ZIBs by restraining the occupation of superfluous zinc metal. In the following content, we mainly review the design fundamentals and recent progress of zinc metal-free anode "rocking chair" ZIBs from the aspects of transition metal dichalcogenides, transition metal oxides, organic compounds, and other materials.

3.1. Transition metal dichalcogenides

As a promising material, transition metal dichalcogenides (TMDs) have been extensively studied for their applications in various energy-related fields [71,72]. TMDs are composed of transition metals (M) and sulfides (X) and are generally considered to be inorganic analogues of graphite. The stoichiometric composition of each TMD layer is MX_2, its central layer is composed of M atoms, and the middle layer is composed of two layers of X atoms. Therefore, each TMD layer can be deemed to be three-atoms thick (X–M–X configuration). One of the interesting features of TMD is the interlayer bond between the two X–M–X layers; weak van der Waals interactions are usually responsible for keeping the structure in place [72]. The presence of such interlayer bonding enables the exfoliation of the bulk TMD into monolayer or few-layer TMD [73]. Furthermore, owing to this distinct 2D structure, the interlayer spacing of TMDs can accommodate intercalated ions. This finding is especially true for battery technologies that use larger hydrated Zn ions, known as ZIB.

Li *et al.* prepared a novel pre-sodiumized titanium disulfide ($Na_{0.14}TiS_2$) and used it as an anode for ZIBs [69]. The introduction of Na can greatly enhance the Zn storage performance of TiS_2. This $Na_{0.14}TiS_2$ anode exhibits a reversible capacity of 140 mAh/g at 50 mA/g with an appropriate discharge potential of 0.3 V (*vs.* Zn^{2+}/Zn) in the electrolyte of 2 mol/L $Zn(CF_3SO_3)_2$; it retains a capacity retention of 98% after 700 cycles at 0.2 A/g and 77% after 5000 cycles at 0.5 A/g. The results of constant current batch titration, X-ray diffraction, scanning electron microscopy, transmission electron microscopy, X-ray photoelectron spectroscopy and density functional theory calculations showed that the TiS_2 presodium that formed $Na_{0.14}TiS_2$ phase not only serves as a buffer phase to enhance the reversibility and stability of the structure, but also the Zn^{2+} ion transfer ability. Consequently, an aqueous "rocking chair" Zn-ion full cell is constructed by combining $Na_{0.14}TiS_2$ anode with $ZnMn_2O_4$ cathode, achieving a capacity of 105 mA/g

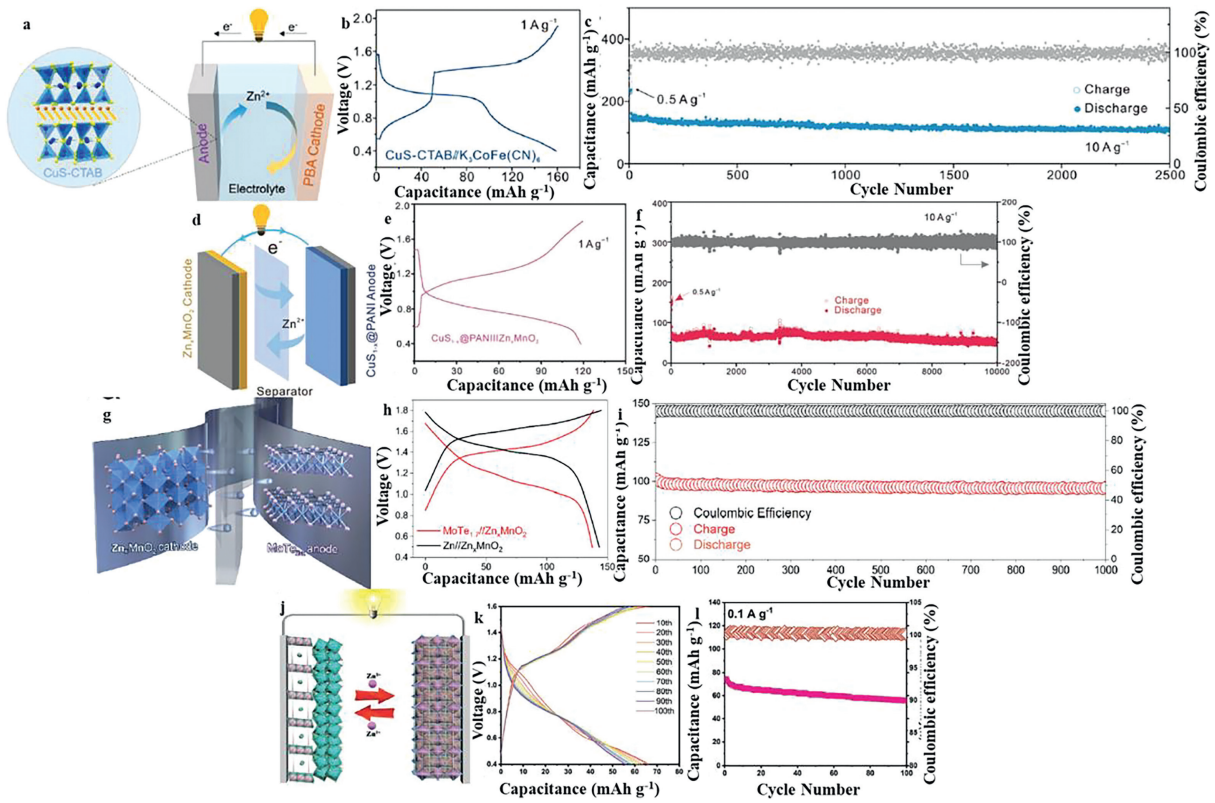

Fig. 3. (a) Schematic illustration, (b) galvanostatic discharge–charge profiles, (c) long-term cycling capability of a CuS-CTAB||$Zn_xFeCo(CN)_6$ full battery. Reproduced with permission [76]. Copyright 2021, The American Chemical Society. (d) Schematic illustration, (e) the charge–discharge profile, (f) long-term cycling performance of the CuS_{1-x}@PANI||Zn_xMnO_2 full battery at 10 A/g. Reproduced with permission [77]. Copyright 2022, Wiley-VCH. (g) Schematic illustration, (h) the charge–discharge profile, (i) long-term cycling performance for the $MoTe_{1.7}$//Zn_xMnO_2 battery. Reproduced with permission [79]. Copyright 2022, Elsevier. (j) Schematic illustration, (k) the charge–discharge profile curves, (l) long cycling stabilities of $Na_{1.6}TiS_2/CuSe_2$//$Zn_xMn_2O_4$ full batteries. Reproduced with permission [81]. Copyright 2022, Wiley-VCH.

with an average voltage of 0.95 V at 0.05 A/g and 74% capacity retention after 100 cycles at 0.2 A/g. Yang *et al.* reported a highly reversible "rocking chair" ZIB, which was composed of a mixed-valence $Cu_{2-x}Se$ anode and a commercial MnO_2 cathode [74]. $Cu_{2-x}Se$ is used as the anode, which simultaneously solves the problems of Zn dendrite growth and electrolyte decomposition in traditional metal zinc anodes. The results show that the incorporation of low-valence copper alters the storage active site of Zn^{2+} ions, thus enhancing the electronic interaction between the active site and the intercalated Zn^{2+} ions, resulting in an intercalation generation energy of −0.68 eV and a decrease in the diffusion barrier. Measurements by *ex-situ* transmission electron microscopy, *ex-situ* X-ray diffraction, and constant-current batch titration techniques revealed that Zn^{2+} can intercalated/extracted reversibly in $Cu_{2-x}Se$ through an intercalation reaction process. The $Cu_{2-x}Se$ nanorod anode is highly advantageous due to its rigid host structure and easy Zn^{2+} diffusion kinetics, exhibiting a CE of approximatively 99.5%, excellent rate capability and long-term cycling stability. The as-constructed Zn_xMnO_2||$Cu_{2-x}Se$ Zn-ion full cell delivers an excellent electrochemical capability, specially a long cycling stability of over 20000 cycles at 2 A/g. Zhao *et al.* developed a secure and eco-friendly Zn-ion micro-battery (ZIMB) by utilizing an MXene-TiS_2 (de)intercalated anode, a multiwalled carbon nanotubes–vanadium dioxide (B) (MWCNTs–VO_2 (B)) cathode, a Zn sulfate–polyacrylamide ($ZnSO_4$–PAM) hydrogel electrolyte and a self-healing polyurethane protective shell construct [75]. This ZIMB exhibits excellent electrochemical capacity with a capacity of 40.8 μAh/cm^2, maximum power density of 32.5 μWh/cm^2 and maximum energy density of 1.2 mW/cm^2. Furthermore, the ZIMB also delivers the good thermostability, flexibility, and self-healability; it can withstand high bending angles of up to 150°, high temperatures of 100 °C, and multiple damage and repair cycles without any significant loss of capacity. Zhang *et al.* designed a conversion reaction anode for ZIBs composed of copper sulfide (CuS) and hexadecyltrimethylammonium bromide (CTAB) superlattices (Fig. 3a) [76]. Owing to the long-chain molecules of CTAB (2.6 nm) and the positively charged head group CTAB ($C_{19}H_{42}N^+$), this superlattice can expand the interlayer spacing by 2.4 nm (001) planes, thus resulting in a charge redistribution that weakens the Coulomb repulsion force and facilitates the diffusion of Zn^{2+}. In addition, CTAB layers can maintain structural stability as interlayer pillars. The high reactivity of Cu ions makes them favorable for growing into larger Cu particles, and this conversion process is accompanied by volume expansion. The CTAB spacer can alleviate the tension, preclude the coalescing of Cu nanoparticles, and ensure the capability to reverse the conversion reaction. As a result, CuS-CTAB exhibits remarkable rate capacity of 225.3 mAh/g at 0.1 A/g with 144.4 mAh/g at 10 A/g and a good cycling stability of 87.6% capacity retention over 3400 cycles at 10 A/g. Furthermore, the full cells are fabricated with a CuS-CTAB superlattice anode and a Prussian blue analogue (PBA, $Zn_xFeCo(CN)_6$) cathode to exhibit a good specific capacity of 159.7 mAh/g at 1 A/g and long cycling stability of 3000 cycles at 10 A/g (Figs. 3b and c). Lv *et al.* proposed CTMAB (hexadecyltrimethylammonium bromide) pre-intercalated CuS (CuS@CTMAB) with expanded interlayer spacing as a anode material for rocking-chair ZIBs (Fig. 3d) [77]. The CTMAB molecule has a strong columnar structure, which can expand the interlayer spacing of CuS, thereby facilitating the intercalation of Zn^{2+}. DFT calculations and *ex-situ* Raman, XRD, TEM and XPS characterizations indicate that CuS@CTMAB undergoes a

typical stepwise intercalation conversion reaction route during discharge. The combination of coefficients of intercalation and switching reaction mechanisms enable not only achieve large Zn^{2+} storage capacity, but also moderate structural transformation and good electron conduction during cycling, resulting in good cycling stability and high-rate performance. Accordingly, the CuS@ CTMAB anode with the appropriate working potential of approximately 0.37 V (*vs.* Zn^{2+}/Zn) exhibits an excellent reversible capacity of 350.3 mAh/g at 0.2 A/g and good cycle life of 99.88% capacity retention over 3000 cycles. Additionally, the CuS@CTMAB||MnO_2 full battery exhibits a high reversible capacity of 78.5 mAh/g with a good capacity retention of 93.9% over 8000 cycles at 2 A/g. Furthermore, the CuS@CTMAB||$CoFe(CN)_6$ Prussian blue full battery can achieve a high average working voltage of 1.05 V (Figs. 3e and f). Lei *et al.* employed *in situ* molecular engineering techniques to fabricate a novel synthetic CuS_{1-x}@polyaniline (PANI) anode for AZIBs, which was Zn-free and could generate appropriate S-vacancies and PANI heterointerfaces simultaneously [78]. The CuS_{1-x}@PANI composite, due to the suitable S-vacancies and unique PANI heterointerface structure, exhibits excellent electrochemical storage performance of Zn^{2+}. The sulfur vacancies not only provide the number of active sites for the storage of Zn^{2+}, but also make the nearby sulfur atoms more amenable to charge transfer, thereby enhancing the storage capacity of Zn^{2+}. In addition, the conductive polymer heterointerface enhances the electrical conductivity, facilitates the transport of ions, and ensures excellent structural stability. The DFT calculation results fully demonstrate the synergistic effect of sulfur vacancies and heterointerface engineering on the whole performance of CuS anodes. As a result, the CuS_{1-x}@PANI half-cell delivers a good capacity of 215 mAh/g at 0.1 A/g and satisfying cycling stability of 90.7 mAh/g after 2000 cycles at 10 A/g. Utilizing HR-STEM images, Operando SXRD, and Operando XAFS spectroscopic characteristics indicate that the storage mechanism of Zn^{2+} is based on the crystalline-amorphous transformation of CuS and a highly reversible transformation reaction. Furthermore, the as-constructed CuS_{1-x}@PANI||Zn_xMnO_2 full cell delivers a high capacity of 138 mAh/g at 1 A/g and displays long cycling stability up to 10000 cycles with a capacity retention of 80% at 10 A/g. Du *et al.* proposed to use $MoTe_{1.7}$ containing tellurium vacancies (TVs) obtained by laser reduction as the anode to prepare Zn-free aqueous ZIBs (Fig. 3g) [79]. According to first-principles calculations, predict that TVs Zn^{2+} can be stored in TVs, which can buffer volume changes, lower the diffusion barrier, and narrow the band gap. By using laser irradiation in experiments, hydrated electrons can be generated in polar solvents to reduce $MoTe_2$, resulting in charge imbalance that leads to the formation of TVs. The results show that the conductivity, capacity, stability, and diffusion kinetics of the electrodes are enhanced by laser irradiation of TVs. The laser-reduced $MoTe_{1.7}$ anode exhibits a good reversible capacity of 338 mAh/g at 0.2 A/g, excellent CE of 100% at 0.2 A/g, and preeminent cycle life of 96% retention for 10,000 cycles at 1 A/g. Moreover, results of both *in situ* diffraction and *ex situ* spectroscopic experiments demonstrated that the capacity of $MoTe_{1.7}$ to store Zn is a conversion reaction at the Mo redox center, involving the formation and dissociation of ZnTe. Furthermore, the $MoTe_{1.7}$||Zn_xMnO_2 pouch-type full cell exhibits an excellent energy density of 137 Wh/kg and high capacity retention of 95% over 1000 cycles (Figs. 3h and i). Du *et al.* reported a layered $TiTe_2$ synthesized by a one-step vacuum sintering method as a metal-free anode for ZIBs [80]. Through *ab initio* molecular dynamics simulations and density functional theory calculations indicated that the $TiTe_2$ electrode through conversion of chemical reactions can deliver a low diffusion energy barrier of approximately 0.23 eV, a fast Zn migration channel with a high diffusion coefficient of 4.7 eV $\times 10^{-11}$ cm^2/s, and high thermodynamic stability. The $TiTe_2$ electrode in the half cell presents a low charging voltage of approximately of 0.7 V in comparison to Zn^{2+}/Zn, a good reversible capacity of 225 mAh/g at 0.1 A/g, and excellent cycling stability of 95% capacity retention over outstanding long life of 30000 cycles at 5 A/g. Additionally, the $TiTe_2$||$Zn_xCo_3O_4$ pouch-type full cell exhibits a satisfying energy density of 149 Wh/kg and excellent capacity retention of 94% after 5000 cycles. Moreover, *in situ* diffraction and *ex situ* spectroscopy indicate that the maintained good reversible capacity of ZnTe depends on the transformation chemistry during the formation and dissociation of ZnTe with Ti^{2+}/Ti^{4+} two-electron redox charge compensation. Cai *et al*. developed an advanced ultrastable aqueous-phase rocking-chair ZIB with dual electric field *in situ* induced insertion/conversion dual-mechanism $Na_{1.6}TiS_2/CuSe_2$ hetero-interfacial anode (Fig. 3j) [81]. The rational structure of the large heterointerface between different phases generates a built-in electric field, which reduces the energy barrier for ion migration, promotes electron and ions diffusion, reduces charge transfer resistance, and establishes a good conduction network. The improved interaction between different atoms at the phase interface relieves the tensile strain, stabilizes the lattice, and achieves good Zn^{2+} diffusion kinetics. The dual-mechanism $Na_{1.6}TiS_2/CuSe_2$ heterostructures can achieve a discharge capacity of 142 mAh/g at 0.2 A/g. Even after a high current evaluation of 10 A/g, this material maintains a discharge capacity of 133 mAh/g at 0.2 A/g current density, displaying an impressive capacity retention of 83.8% at 5A/g over 12000 cycles (Figs. 3k and l).

Although transition metal dichalcogenides have shown great potential in rocking-chair ZIBs, they are currently limited to TiS_2 and CuS-based dichalcogenides materials. Therefore, suitable transition metal dichalcogenide materials should be found for "rocking chair" ZIBs in the follow-up research.

3.2. Transition metal oxides

Transition metal oxides are considered very attractive battery candidates because of their excellent reversible capacity, as well as eco-friendliness, corrosion resistance, and good cost economy [82]. In addition, the higher potential and higher safety of intercalated alkali metal ions are another advantage of transition metal oxide [83]. Likewise, transition metal oxides have also shown great potential for Zn ion storage.

Xiong *et al.* proposed hexagonal MoO_3 (h-MoO_3) as an intercalated anode as an alternative electrode for Zn metal plates (Fig. 4a) [84]. The energy storage mechanism of h-MoO_3 is related to the primary intercalation and extraction of H_2O and Zn^{2+}, the secondary intercalation and extraction of SO_4^{2-}, and the reversible exchange of NH_4^+. Taking advantage of its hexagonal structure, h-MoO_3 exhibits a good capacity of 120 mAh/g at 0.2 A/g, and maintains an excellent capacity retention of 99% after 100 cycles at 0.3 A/g, further demonstrating its excellent cycling stability. Moreover, a Zn metal-free full battery with h-MoO_3 anode and a $Zn_{0.2}MnO_2$ cathode exhibits a specific capacity of 56.7 mAh/g at energy density of 61 Wh/kg and an exceptional capacity retention of 100% after 1000 cycles (Figs. 4b and c). Wang *et al*. employed a hydrothermal method to fabricate monoclinic MoO_x and use it as the anode for ZIBs [85]. The as-prepared monoclinic MoO_x delivered high discharge/charge capacities of 53.3/53.1 mAh/g and ideal average potential of 0.53 V (*vs.* Zn^{2+}/Zn) at high current density of 10 A/g between 0.1 V and 1 V, high discharge/charge capacities of 82.5/82.0 mAh/g at 10 A/g, and eventually discharge/charge capacities of 44.4 mAh/g after 30000 cycles. In addition, the cyclic voltammetry technique was utilized to analyze the kinetic behavior of the Zn ion storage process of monoclinic MoO_x. Results demonstrate that, at high scan rates, the electrochemical reaction process is mainly driven by capacitive contributions, thus exhibiting excellent rate characteristics of monoclinic MoO_x at high current densities. The storage mechanism of zinc ions was investigated by X-ray diffrac-

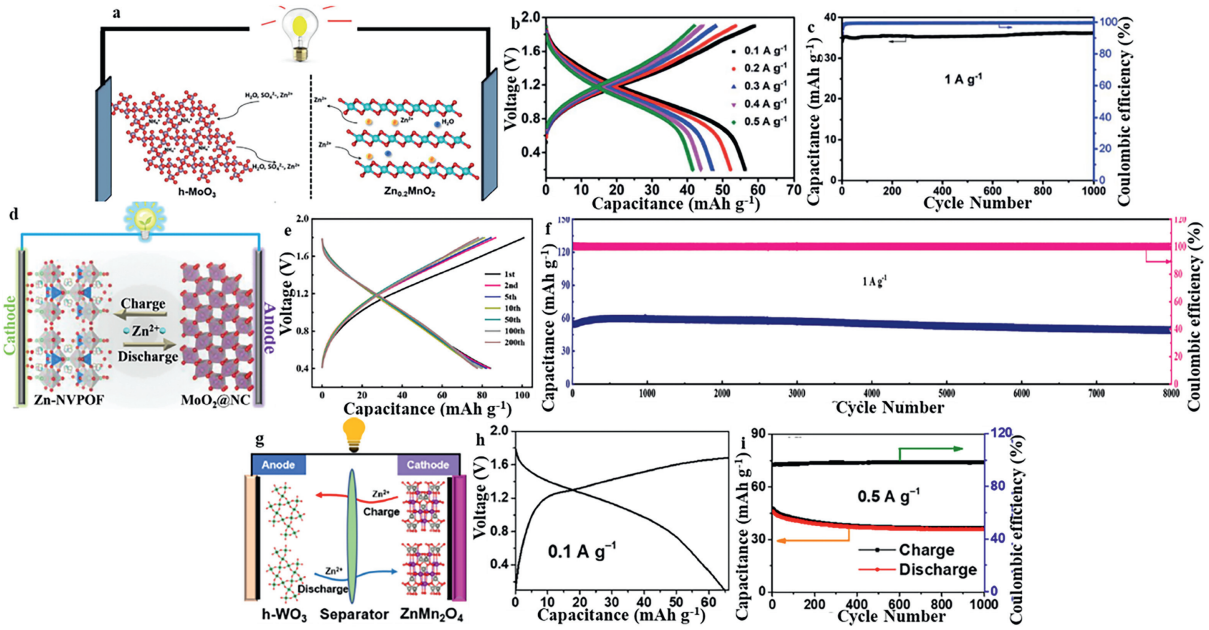

Fig. 4. (a) Schematic illustration, (b) the charge and discharge curves, (c) cycling performance of the h-MoO_3//$Zn_{0.2}MnO_2$ battery. Reproduced with permission [84]. Copyright 2020, The Royal Society of Chemistry. (d) Schematic illustration of MoO_2@NC||Zn-$Na_3V_2(PO_4)_2O_2$ full cell; (e) Typical galvanostatic charge–discharge curves at 0.3 A/g; (f) Long cycling performance at 5 A/g. Reproduced with permission [86]. Copyright 2021, Wiley-VCH. (g) Schematic illustration, (h) typical charge/discharge curves, (i) cycling stability of the h-WO_3/3DG//$ZnMn_2O_4$/carbon black full battery. Reproduced with permission [87]. Copyright 2022, The American Chemical Society.

tion and deduced as: $MoO_x + yZn^{2+} + 2ye^- \rightleftharpoons Zn_yMoO_x$. Furthermore, by comparing the differences of the Zn_δ-MoO_x anode and the metal Zn alone to construct the battery indicated that the former shows significant advantages in electrochemical performance, especially rate capability. Wang *et al.* designed a novel nitrogen-doped carbon intercalation layered MoO_2 (MoO_2@NC) material through a combination of interlayer engineering and *in-situ* carbonization of aniline guests in molybdenum trioxide layers, which is suitable to be used as an intercalated anode for ZIBs (Fig. 4d) [86]. The even dispersion of carbon layers in layered MoO_2 not only provides a fast transport path for electrons, but also strengthens the structure of MoO_2, making it highly structurally integrated during high-speed cycling. The carbon-intercalated MoO_2 electrode displays good initial CE, satisfying cycling stability, and excellent rate capability due to its unique structural design. Multiple *ex situ* characterizations suggest that its good electrochemical stability stems from a reversible intercalation mechanism and an ultrastable structural framework. In addition, the "rocking chair" ZIB assembled with Zn-pre-intercalated $Na_3V_2(PO_4)_2O_2F$ cathode that exhibits good stability and long cycling stability, with a capacity retention rate as high as 91% over 8000 cycles (Fig. 4e and f). Cao *et al.* fabricated a tungsten oxide/tungsten carbide layered hybrid heterostructure (WO_3/WC) with good interfacial energy and strong electronic coupling *via* a convenient calcination technology and employed it as an intercalation anode for rocking chair ZIBs [58]. Stacked and divergent WO_3 nanosheets, featuring multiple active sites and multiple oxidation states, can be employed to storage Zn^{2+}. Meanwhile, both experimental and theoretical investigations show that the combination WO_3 and WC can considerably enhance the electronic and ionic conductivity, which is beneficial to the formation of a thermodynamically stable interface. Consequently, the as-prepared WO_3/WC exhibit excellent capacity at 164 mAh/g at 0.1 A/g and good cycle life of 90.2% over 1000 cycles at 1.0 A/g. Moreover, the assembled WO_3/WC||MnO_2/graphite rocking-chair ZIBs deliver good capacity of 69 mAh/g at 0.1 A/g, excellent cycling stability of 100% after 10000 cycles and satisfying energy density of 85 Wh/kg at 106 W/kg. Chen *et al.* employed a solvothermal method to construct hexagonal WO_3/3D porous graphene (h-WO_3/3DG) as an intercalated anode for ZIBs (Fig. 4g) [87]. The crystal structure of WO_3 in this complex is a hexagonal channel with a diameter of 5.36 Å, which is much large than that of Zn^{2+} (0.73 Å), which accelerates the insertion and extraction of Zn ions. Accordingly, the h-WO_3/3DG||Zn half-cell delivers good electrochemical capability with a satisfying capacity of 115.6 mAh/g at 0.1 A/g and 89% capacity retention at 2.0 A/g after 10000 cycles. Furthermore, a full cell was fabricated with h-WO_3/3DG as the anode and $ZnMn_2O_4$/carbon black as the cathode, without the use of Zn metal, yielding an initial capacity of 66.8 mAh/g at 0.1 A/g, which corresponds to an energy density of 73.5 Wh/kg (based on the total mass of anode and cathode-active materials) and the capacity retention was 76.6% after 1000 cycles at 0.5 A/g (Figs. 4h and i).

Transition metal oxides have been shown to be highly effective electrode materials, as they possess both high specific capacities and rapid electrochemical redox reaction rates. Despite the advantages of zinc storage, transition metal oxides have drawbacks such as slow rate, short cycle life, significant volume expansion, and electrode fracture during charging and discharging. Thus, the actual specific capacity is significantly lower than the theoretical specific capacity. At the same time, transition metal oxides are rarely employed in rocking-chair ZIBs, and currently only focus on materials, such as MoO_2, MoO_3 and WO_3. In the follow-up research, suitable transition metal oxides should be developed for rocking chair ZIBs.

3.3. Organic compounds

Organic materials are seen as some of the most prospective new battery electrode materials due to their potential to be synthesized from green natural resources, as well as their ability to be tuned for performance through molecular design [88,89]. More importantly, in comparison to the strong chemical bonds in inorganic materials and the strong covalent bonds in molecules, the intermolecular interactions of organic compounds are relatively weak, allowing for the storage of large-sized multivalent metal ions in

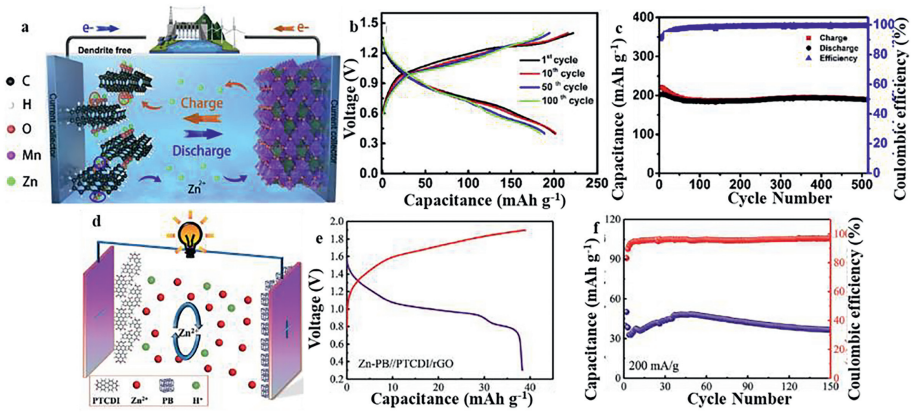

Fig. 5. (a) Schematic illustration, (b) the charge and discharge curves, (c) cycling performance of the 9,10-anthraquinone//$ZnMn_2O_4$ battery. Reproduced with permission [92]. Copyright 2019, Elsevier. (d) Schematic illustration, (e) the charge and discharge curves, (f) cycling performance of the perylene-3,4,9,10-tetracarboxylic diimide/RGO||Prussian blue full cell. Reproduced with permission [93]. Copyright 2020, Wiley-VCH.

the large intermolecular spacing [90,91]. These properties enable the rapid advancement of organic electrodes in ZIBs.

Yan *et al.* adopted Zn dendrite-free organic 9,10-anthraquinone (AQ) to replace metallic Zn to prepare ZIBs (Fig. 5a) [92]. The ZIBs used organic AQ-derived as the anode and 1 mol/L $ZnSO_4$+ 0.05 mol/L $MnSO_4$ aqueous solution as the electrolyte, and the synthesized $ZnMn_2O_4$ was selected as the cathode. The as-assembled ZIBs deliver good cycle life with capacity retention of 94.4%, high specific capacity of 189.5 mAh/g after 500 cycles and a specific energy of 81 Wh/kg (Figs. 5b and c). Liu *et al.* reported that a polymerized version of perylene-3,4,9,10-tetracarboxydiimide (PTCDI) on reduced graphene oxide (PTCDI/rGO) could be used as a dendrite-free anode for zinc-ion batteries (ZIBs) (Fig. 5d) [93]. The as-prepared PTCDI/rGO electrode not only not only enhances the stability of ZIBs by preventing non-uniform Zn stripping and plating, but also offers remarkable rate capability and a long cycling stability, due to the phase transfer mechanism that involves protons and Zn ions (reaching 130 mAh/g at 3 A/g with 97% capacity retention after 1500 cycles). Moreover, the low potential of PTCDI was explained using density functional theory. Furthermore, the full cell constructed with the PTCDI/rGO as anode and commercial Prussian blue as cathode exhibits a high capacity of 193 mAh/g and an appropriate operation voltage of 0.95 V at 0.2 A/g yet retains 75% capacity at 0.2 A/g with the cycle life span of 150 times (Figs. 5e and f). Liu *et al.* reported a scalable 1,4,5,8-naphthalene diimide (NI) as a dendrite-free organozinc anode for ZIBs and investigated the effect of different binders on the electrochemical capability of NI electrodes [94]. The electrochemical performance of NI electrodes prepared with polyvinylidene fluoride (PVDF) binder is not satisfactory, and the stability of the electrode structure is poor. In comparison, the NI electrode with polytetrafluoroethylene (PTFE) as the binder exhibits good rate performance of 122.2 mAh/g at 5 A/g and satisfying cycling stability. The improved stable cycling performance of NI by the PTFE binder is due to its efficient maintenance of the electrode structure during cycling, thereby inhibiting the dissolution of organic molecules. In addition, ion kinetic analysis shows that capacitive charge storage provides superior rate capability. Through *ex situ* Raman spectroscopy and *in situ* attenuated total reflection Fourier transform infrared spectroscopy (ATR-FTIR) revealed that the carbonyl group of nickel is the electrochemically active center. Furthermore, A Zn-ion full battery, employing metal-free NI anode and Prussian blue analogues cathode, is capable of delivering an impressive rate capability of 113.9 mAh/g at 10.0 A/g, good operation voltage of approximately 1.2 V at 1.0 A/g and energy density of 50.2 Wh/kg_{total}. Xu *et al.* synthesized a series of CNT-containing and CNT-free molecules and polymers and employed them as ZIB anodes [95]. Among these materials, a polymer/carbon nanotube hybrid based on perylene 3,4,9,10-tetracarboxydianhydride showed the best electrochemical property. Then, electrolytes containing different concentrations of Zn salts were investigated experimentally and by simulation, and the result showed that the addition of trifluoride, high ionic conductivity, mild acidity, and low viscosity could significantly increase transmission characteristics for fast and stable storage of ions. The optimized combination of the polymer anode will enable the polymer result in a low discharge voltage of 0.2–0.4 V *vs.* Zn^{2+}/Zn, a good capacity of 128 mAh/g at 0.05 mA/g, a high CE of approximately 100%, a high loading of approximately 50 mg/cm^2, fast charging capability of 100 A/g, and extraordinary cycling stability for up to one million cycles. The storage mechanism of this polymer was revealed by *in situ* and *ex situ* characterization and electrochemical measurements, uncovering the mechanism of reversible Zn^{2+} (de-) coordination and proton interaction in the polymer. Moreover, full battery based on the PI-1/CNT anode exhibits a high-power density of 9.1 kW/kg, long cycle life of 50,000 cycles, and cycling stability for over sub-million cycles at 10 and 200 A/g.

In recent years, the design of organic active electrodes has made great progress in rocking chair ZIBs, but much work still needs to be done. Generally speaking, the capacity and voltage of a battery are essential in determining its energy density. Organic materials require intelligent design at the molecular level to avoid the trade-off between high capacity and high voltage. Moreover, organic-inorganic hybrid materials combine the advantages of both inorganic and organic electrode materials, which are beneficial to improve the energy density of electrodes. Furthermore, fine-tuning the chemical structure to tune intermolecular interactions enables to simultaneously control the solubility of the material, retain high capacity, and even increase output voltage.

3.4. Other materials

In addition to the transition metal dichalcogenides, transition metal oxides, and organic compounds were applied to the anode of rocking chair ZIBs. Prussian blue analogs, hydrated titanic acid, hydrated ammonium vanadate, and Te were also applied to rocking chair type ZIBs. Chae *et al.* reported the construction of $Zn_2Mo_6S_8$ as anode and $K_{0.02}(H_2O)_{0.22}Zn_{2.94}[Fe(CN)_6]_2$ (rhombic Prussian blue analog) as cathode in $ZnSO_4$ aqueous electrolyte Rocker-style ZIBs [96]. The full battery delivers a reversible cycle, with a capacity of 62.3 mAh/g and an average discharge cell voltage of 1.40 V. Liu *et al.* adopted hydrated titanic acid ($H_2Ti_3O_7{\cdot}xH_2O$) as the anode material for a novel type of ZIBs with potential properties sim-

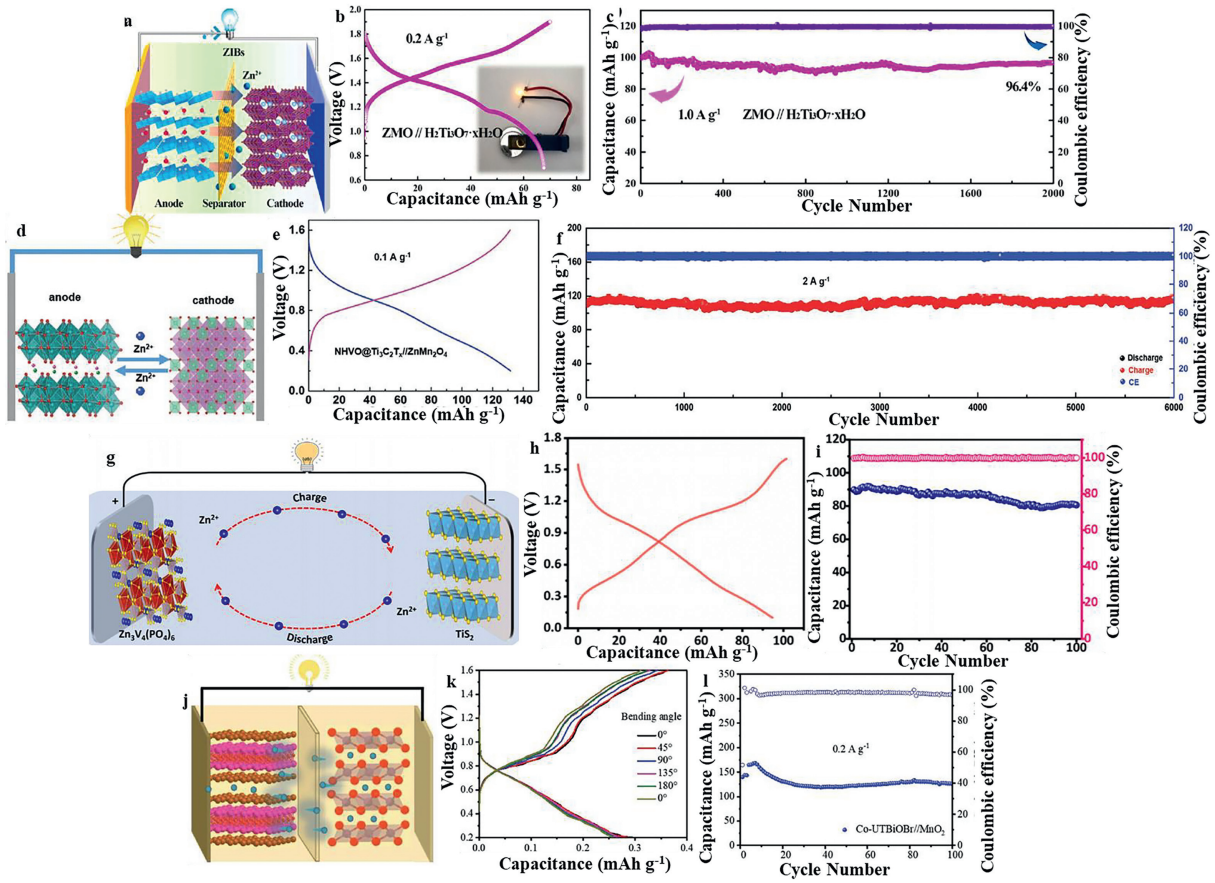

Fig. 6. (a) Schematic illustration, (b) the charge and discharge curves, (c) cycling performance of Zn^{2+} inserted MnO_2//$H_2Ti_3O_7·xH_2O$ full cell. Reproduced with permission [97]. Copyright 2021, Elsevier. (d) Schematic illustration, (e) the charge and discharge curves, (f) cycling performance of $(NH_4)_2V_{10}O_{25}·8H_2O$@$Ti_3C_2T_x$//$ZnMn_2O_4$ full battery. Reproduced with permission [98]. Copyright 2021, Wiley-VCH. (g) Schematic illustration, (h) typical charge/discharge curves, (i) cycling stability of the $Zn_3V_4(PO_4)_6$//TiS_2 full battery. Reproduced with permission [100]. Copyright 2022, Elsevier. (j) Schematic illustration, (k) typical charge/discharge curves, (l) cycling stability of the Co-UTBiOBr//MnO_2 full battery. Reproduced with permission [103]. Copyright 2022, Wiley-VCH.

ilar to TiO_2 and extended interlayer spacing supported by crystalline water (Fig. 6a) [97]. The low potential of $H_2Ti_3O_7·xH_2O$ (0.2 V *vs.* Zn^{2+}/Zn) can significantly improve the working voltage level of Zn-ion full cells. Results of a thorough investigation demonstrate that the increased lattice spacing and interlayer crystal water of the $H_2Ti_3O_7·xH_2O$ anode promote the simultaneous insertion and extraction of Zn^{2+} with H^+. The $H_2Ti_3O_7·xH_2O$ anode with low potential demonstrates excellent cycling capability and CE, thanks to the presence of interlayer crystal water. The assembled Zn_xMnO_2//$H_2Ti_3O_7·xH_2O$ ZIB has good electrochemical capability, specially the output voltage exceeds 1 V (Figs. 6b and c). Wang *et al*. alternately assembled $(NH_4)_2V_{10}O_{25}·8H_2O$ (NHVO) nanoribbons and $Ti_3C_2T_x$ MXene nanosheets in the form of hybrid films to construct NHVO@$Ti_3C_2T_x$ hybrid films and used them as anodes for rocking-chair ZIBs (Fig. 6d) [98]. The as-prepared NHVO nanobelts have ultrathin morphological features, the particle size is only approximately 14 nm, and the dispersibility is good. Through the combination of 2D $Ti_3C_2T_x$ nanosheets, a flexible NHVO@$Ti_3C_2T_x$ hybrid film electrode was achieved and exhibited fast ion and electron transmission. Benefiting from the crystal structure advantage of NHVO and the auxiliary role of $Ti_3C_2T_x$ nanosheets, the NHVO@$Ti_3C_2T_x$ hybrid film electrode achieves a good capacity of up to 514.7 mAh/g and excellent cycling stability of 84.2% capacity retention at 5.0 A/g after 6000 cycles. Furthermore, a "rocking chair" Zn ion full cell composed of NHVO@$Ti_3C_2T_x$ as anode and $ZnMn_2O_4$ as cathode exhibits the highest specific capacity of 131.7 mAh/g (based on total mass), the largest energy density of 97.1 Wh/kg, and excellent cycling stability of 92.1% after 6000 cycles at 2.0 A/g (Figs. 6e and f). Chen *et al*. replaced metallic Zn with the chalcogen tellurium (Te) to prepare a switching tellurium-based ZIBs that can operate in mild and alkaline electrolytes [99]. The different transformation mechanisms of mild electrolyte (Te→$ZnTe_2$→ZnTe) and alkaline electrolyte (TeO_2→Te→ZnTe) were confirmed by XRD and XPS characterization. Dendrites and HER are complete eliminated, with good cycle life in mild and alkaline electrolytes (over 5000 cycles with a high-capacity retention over 75%), owing to advanced switching mechanisms. Additionally, with appropriate N/P ratio, high capacity and high energy density can be obtained in the Te/MnO_2 (106 mAh/g anode + cathode and 81 Wh/kg anode + cathode) and Te/$Ni(OH)_2$ (161 mAh/g anode + cathode and 176.3 Wh/kg anode + cathode) batteries with high utilization of anode (up to 50.1% and 38.9%, respectively). Zhang *et al*. concluded that the layered BiOI has a suitable interlayer distance (0.976 nm) and a low Zn^{2+} diffusion barrier (0.57 eV) based on density functional theory, and designed free-standing BiOI nanopaper as an anode for ZIBs [100]. The intercalation process and mechanism of $Zn(H_2O)_n^{2+}$ in BiOI were confirmed by means of ultra-*in situ* X-ray diffraction, Raman spectroscopy and X-ray photoelectron spectroscopy. The potential of BiOI nanopaper as a superior anode is demonstrated by its suitable potential (0.6 V *vs.* Zn/Zn^{2+}), satisfying reversible capacity (253 mAh/g), excellent rate performance (171 mAh/g at 10 A/g), stable cycling performance (113 mAh/g after 5000 cycles at 5 A/g), and dendrite-free operation. The *quasi*-solid-state battery, composed of BiOI nanopa-

per anode and Mn_3O_4 cathode, displays a high initial capacity of 149 mAh/g (for anode) and an excellent capacity retention of 70 mAh/g after 400 cycles. The self-assembled flexible battery also exhibits good cycling stability in flexible electrochemical tests. Zhao *et al*. developed a stable "rocking chair" ZIB using a low-strain (2.4% volume change) $Zn_3V_4(PO_4)_6$ (ZVP) cathode and layered TiS_2 anode (Fig. 6g) [101]. The as-prepared ZVP/rGO cathode offers a reversible capacity of 105.2 mAh/g with a high operating voltage of 1.5 V (*vs*. Zn^{2+}/Zn), excellent cycle life of 100% capacity retention over 250 cycles and good rate performance of 90.6 mAh/g at 10 C and 62.9 mAh/g at 40 C in a half cell. *In situ* Raman, *in situ* XPS and XRD characteristics indicated that the ZVP cathode possesses reversible Zn intercalation and deintercalation reactions and structural stability. The DFT calculation results show that the two Zn^{2+} sites on the Zn^{2+} sites can be extracted reversibly, confirming that the volume of ZVP changes slightly during Zn^{2+} storage. Furthermore, the "rocking chair" ZVP//TiS_2 full cell delivers good electrochemical reversibility and cycling capability (Figs. 6h and i). Zhao *et al*. synthesized a novel rocking chair type ZIB cathode material, $Zn_3V_4(PO_4)_6$@C (ZVP@C), and evaluated its electrical conductivity using a composite carbon coating [102]. By taking advantage of the two-electron reaction of vanadium and the co-intercalation of Zn^{2+}/H^+, ZVP@C/30%BP displays a specific capacity reach up to 120 mAh/g at 0.04 A/g and an excellent capacity retention of 80% after 400 cycles at 1 A/g. Long *et al.* fabricated few-atom layered co-doped BiOBr nanosheets (Co-UTBiOBr) by a one-step hydrothermal process, and designed freestanding flexible electrodes composed of Co-UTBiOBr and CNTs (Fig. 6j) [103]. Ultrathin nanosheets consisting of three atomic layers and carbon nanotubes facilitate the transfer of Zn^{2+} and electrons respectively, respectively. It has been established through experimental and theoretical studies that co-doping is advantageous in lowering the diffusion barrier of Zn^{2+}, increasing the volume expansion after Zn^{2+} intercalation, and enhancing the electronic conductivity of BiOBr. Based on the *ex situ* characterization, an insertion transition mechanism is proposed. Profiting from many advantages, Co-UTBiOBr delivers a satisfying capacity of 150 mAh/g at 0.1 A/g and an excellent cycling stability of 100% capacity retention after 3000 cycles at 1 A/g. Especially, outstanding electrochemical capabilities was retained even at an ultrahigh mass loading of 15 mg/cm^2. Co-UTBiOBr//MnO_2 "rocking chair" ZIB delivers a stable cycling performance of 130 mAh/g at 0.2 A/g during cyclic test and its flexible quasi-solid-state battery exhibits excellent stability when bent in various forms (Figs. 6k and l).

The development of diverse anode materials for rocking chair ZIBs is one of the main factors hindering their industrialization. Therefore, the search for anode materials for rocking chair ZIBs should be expanded in subsequent studies.

4. Summary and outlook

In conclusion, the novel Zn-free metal rocking chair type ZIBs may offer a new solution to the for a long-time challenge of Zn metal anodes. The higher working potential of zinc metal-free anodes, which can effectually prevent side reactions and inhibit the formation of Zn dendrites, improves safety and service life. However, the limited energy density has yet to be enhanced, and Zn metal anodes may be the ultimate solution. Thus, in this review, the recent research progress of zinc metal-free anode materials (transition metal dichalcogenides, transition metal oxides, organic compounds, and other materials) for "rocking chair" type ZIBs is reviewed (Table 1). The comparison of transition metal dichalcogenides, transition metal oxides and organic compounds materials shows that transition metal dichalcogenides-based composites exhibit excellent specific capacity and cycling performance in ZIBs. Meanwhile, like some $(NH_4)_2V_{10}O_{25}{\cdot}8H_2O$@$Ti_3C_2T_x$ composites exhibit higher specific capacitance and cycling performance. Despite the many advantages of rocking chair ZIBs, research on them is only beginning. Here, we put forward some views and suggestions in this field as follows:

(1) Defects and composites are effective ways to improve zinc-free metal anode materials. The practical application of rocking chair type ZIBs is mainly hindered by the strong electrostatic interaction between conventional anode materials and divalent Zn^{2+}, leading to irreversible and severe structural damage, unsatisfactory cycling stability and poor multiplicative performance. The introduction of a defect can reduce the diffusion potential barrier and thus improve the diffusion kinetics. In addition, defect sites can act as active sites for storing guest ions, providing additional capacity to the electrode. Moreover, the introduction of anionic vacancies (*e.g.*, oxygen and sulfur vacancies) is always accompanied by charge compensation of the cation mixed-valence state, enhancing the electrical conductivity. Furthermore, when compounded with a highly conductive material, it exhibits rapid ion and electron transfer, resulting in excellent zinc storage performances.

(2) Novel long cycle life and high energy zinc metal-free anodes (such as alloy-type mechanisms, conversion-type, and insertion-type) remain to be explored. The new alloy anode has the advantages of good electrical conductivity, large theoretical specific capacity, and low working potential; it is expected to become a development direction of various rechargeable metal-ion batteries. Alloy-type materials possess the advantages of high theoretical specific capacity and low operating voltage, making them potential anode materials for rocking chair ZIBs. As of yet, no alloy-based anodes have been studied in relation to zinc-free metal rocking chair ZIBs. Additionally, extensive research into conversion and insertion anodes for high-performance rocking chair ZIBs is highly encouraged.

(3) The storage mechanism of Zn requires to be thoroughly and systematically explored by combining theoretical research with experiment. The theoretical simulation calculation can provide a basis for the screening and exploration of rocking chair ZIBs materials. The exploration and comprehension of the fundamental science that supports applied research, such as the redox potential of Zn^{2+}, the LUMO and HOMO energy levels, the Zn^{2+} diffusion barriers, diffusion efficiencies, ion transport pathways, and volume expansion, are essential for the discovery and optimization of high-performance electrodes. It is possible to anticipate structural stability, thus providing fundamental understanding of the selection and power of zinc metal-free anodes that have been reduced in size. Potential energy-based methods, such as atomic static lattice, molecular dynamics methods and electronic structure methods (DFT, Hartree-fock) can offer theoretical guidance for future research. On the other contrary, experimental measurements can actually study the electrochemical behavior during charge and discharge (such as redox potential, cycling stability and diffusion coefficient) and structural changes. Electrochemical measurements (such as charge–discharge curves, CV curves and GITT curves) and various spectra (such as *in-situ* and *ex-situ* XRD, Raman, Fourier transform infrared spectroscopy, XPS and TEM) can explore interface features, intermediates, and failure mechanisms.

(4) The pairing of Zn-rich cathodes with zinc metal-free anodes requires further exploration and research. Despite the abundance of works based on these cathodes, their inherently weak conductivity, unsatisfied cycling capability, and

Table 1
Comparison of the reported ZIBs based on "rocking chair" type with zinc-free metal anodes (The data in the table are based on measurements of coin cells).

Anode materials	Devices (anode//cathode)	Voltage window (V)	Electrolyte	Cycle performance	Specific capacitance (mAh/g)	Refs.
Transition metal dichalcogenides	$Na_{0.14}TiS_2$//$ZnMn_2O_4$	0.05-1.0	4 mol/L $Zn(CF_3SO_3)_2$	74%, 100 cycles, 0.2 A/g	140	[69]
	$Cu_{2-x}Se$//Zn_xMnO_2	0.4-1.6	1 mol/L $ZnSO_4$	99.9%, 20000 cycles, 2 A/g	200.5	[74]
	MXene-TiS_2// MWCNTs-VO_2(B)	0.05-1.0	2 mol/L $ZnSO_4$	99.7%, 500 cycles, 2 A/g	172	[75]
	CuS-CTAB// $Zn_xFeCo(CN)_6$	0.2-1.6	4 mol/L $Zn(CF_3SO_3)_2$	78.5%, 2500 cycles, 2 A/g	230.6	[76]
	CuS@CTMAB// Zn^{2+}-MnO_2	0.8−1.8	2 mol/L $ZnSO_4$ + 0.1 mol/L $MnSO_4$	93.9%, 8000 cycles, 2 A/g	167.4	[77]
	CuS_{1-x}@PANI//Zn_xMnO_2	0.2–1.2	3 mol/L $ZnSO_4$+0.1 mol/L $MnSO_4$	80%, 10000 cycles, 0.5 A/g	138	[78]
	$MoTe_{1.7}$//Zn_xMnO_2	0.5-1.8	3 mol/L $Zn(CF_3SO_3)_2$	96%, 10000 cycles, 1 A/g	338	[79]
	$TiTe_2$//ZnxCo$_3O_4$	0.5-2.0	1 mol/L $ZnSO_4$ + 0.1 mol/L $MnSO_4$	94%, 5000 cycles, 1 A/g	225	[80]
	$Na_{1.6}TiS_2$/$CuSe_2$// $Zn_xMn_2O_4$	0.4-1.6	1 mol/L $ZnSO_4$ + 0.5 mol/L $MnSO_4$	79%, 100 cycles, 0.1 A/g	125.6	[81]
Transition metal oxides	h-MoO_3//$Zn_{0.2}MnO_2$	0.2-1.9	1 mol/L $ZnSO_4$	100%, 1000 cycles, 1 A/g	56.7	[84]
	MoO_x//Zn_δ-MoO_x	0.1-1.0	2 mol/L $ZnSO_4$ + 0.2 mol/L $MnSO_4$	84%, 50 cycles, 0.05 A/g	82.5	[85]
	MoO_2@NC//Zn-$Na_3V_2(PO_4)_2O_2F$	0.4-1.8	1 mol/L $ZnSO_4$	91%, 8000 cycles, 1 A/g	158	[86]
	WO_3/WC// MnO_2/graphite	0.2-1.8	1 mol/L $ZnSO_4$	100%, 10000 cycles, 1 A/g	69	[58]
	h-WO_3/3DG// $ZnMn_2O_4$/CB	0.2-1.8	3 mol/L $Zn(CF_3SO_3)_2$	76.6%, 1000 cycles, 0.5 A/g	62.3	[87]
Organic compounds	9,10-Anthraquinone// $ZnMn_2O_4$	0.4-1.4	1 mol/L $ZnSO_4$ + 0.05 mol/L $MnSO_4$	99.4%, 500 cycles, 0.2 A/g	190.4	[92]
	PTCDI/rGO//Prussian blue	0.8-1.9	2 mol/L $ZnSO_4$	75%, 100 cycles, 1 A/g	193	[93]
	NI//KZnHCF	0.1-1.9	1.5 mol/L $Zn(CF_3SO_3)_2$	70%, 120 cycles, 0.1 A/g	113.9	[94]
	PI-1/CNT//ZnxMnO_2	0.1-1.8	1.5 mol/L $Zn(CF_3SO_3)_2$	96%, 6000 cycles, 2 A/g	150	[95]
Other materials	$Zn_2Mo_6S_8$//ZPB	1.1-2.1	0.1 mol/L $ZnSO_4$	-	62.3	[96]
	$H_2Ti_3O_7 \cdot xH_2O$//ZMO	0.7-1.9	1 mol/L $ZnSO_4$+ 0.1 mol/L $MnSO_4$	92.4%, 2000 cycles, 1 A/g	67	[97]
	NHVO@$Ti_3C_2T_x$// $ZnMn_2O_4$	0.8-1.8	3 mol/L $Zn(CF_3SO_3)_2$	92.1%, 6000 cycles, 2 A/g	498.4	[98]
	Te//$Ni(OH)_2$	0.1-1.7	0.3 mol/L $Zn(CF_3SO_3)_2$	50.1%, 300 cycles, 1 A/g	161	[99]
	BiOI//Mn_3O_4	0.1-1.4	2 mol/L $Zn(CF_3SO_3)_2$	47%, 400 cycles, 0.5 A/g	149	[100]
	TiS_2//$Zn_3V_4(PO_4)_6$	0.1-1.6	1 mol/L $ZnSO_4$	93.8%, 100 cycles, 0.1 A/g	94.6	[101]
	$Zn_3V_4(PO_4)_6$@C// Prussian blue	0-1.9	2 mol/L $ZnSO_4$	92.1%, 45 cycles, 0.04 A/g	120	[102]
	Co-UTBiOBr//MnO_2	0.2-1.6	2 mol/L $Zn(CF_3SO_3)_2$	96.3%, 159 cycles, 1 A/g	130	[103]

Acronym definitions: perylene-3,4,9,10-tetracarboxylic diimide (PTCDI) polymerized on the surface of reduced graphene oxide (PTCDI/rGO), 1,4,5,8-naphthalene diimide (NI), $K_x(H_2O)_{0.22}Zn_3[Fe(CN)_6]_2$ (ZPB), Zn^{2+} inserted MnO_2 (ZMO), $(NH_4)_2V_{10}O_{25}\cdot 8H_2O$@$Ti_3C_2T_x$ (NHVO@$Ti_3C_2T_x$).

capacity retention are still inadequate and require further advancement. Various strategies (such as defect engineering, recombination and doping) can be employed to improve redox voltage, stabilize output voltage, maintain capacity retention, and lengthen cathode stability. In addition, new cathodes with excellent capacity and high voltage should be conducted to explored.

(5) In-depth research on the development of advanced electrolytes for rocking chair ZIBs is necessary. The electrolyte has a greatly influences on the stability of the electrode and electrolyte interface, CE, chemical and electrochemical stability of the electrode, ion migration, Zn^{2+} migration number, and voltage window, and then ultimately affects the electrochemical capability of the ZIBs. Despite a variety of excellent performance electrolytes such as aqueous electrolytes, organic electrolytes, hydrogel electrolytes, and solid-state electrolytes have obtained good electrochemical performance in ZIBs, advanced electrolytes, such as ionic liquids, saline electrolytes, or solid-state electrolytes, deserve considerable concern. Unfortunately, few investigations on electrolytes dedicated to rocking chair ZIBs has been conducted. In addition, the cathode mass ratio, separator, current collector, cell configuration, temperature, and pressure affect the electrochemical capability of the final rocking chair ZIB. These factors should also be systematically considered.

Declaration of competing interest

The authors declare that they have no known competing financial interests or personal relationships that could have appeared to influence the work reported in this paper.

Acknowledgments

This work was supported the National Natural Science Foundation of China (No. 62101296), the Natural Science Foundation of Shaanxi Province (Nos. 2021JQ-760 and 2021JQ-756).

References

[1] B. Obama, Science 355 (2017) 126–129.
[2] S. Carley, D.M. Konisky, Nat. Energy 5 (2020) 569–577.
[3] W.P. Schill, Joule 4 (2020) 2059–2064.
[4] D. Zhang, L. Li, W. Zhang, et al., Chin. Chem. Lett. 34 (2022) 107122.
[5] D. Zhang, C. Tan, T. Ou, et al., Energy Rep. 8 (2022) 4525–4534.
[6] L. Li, D. Zhang, J. Deng, et al., Carbon 183 (2021) 721–734.
[7] L. Li, W. Zhang, W. Pan, et al., Nanoscale 13 (2021) 19291–19305.

[8] J. Zheng, Z. Huang, F. Ming, et al., Small 18 (2022) 2200006.
[9] J. Cao, D. Zhang, X. Zhang, et al., Energy Environ. Sci. 15 (2022) 499–528.
[10] Z. Liu, Y. Huang, Y. Huang, et al., Chem. Soc. Rev. 49 (2020) 180–232.
[11] Y. Tian, Y. An, C. Liu, et al., Energy Storage Mater. 41 (2021) 343–353.
[12] D. Chao, F. Xie, C. Ye, et al., Sci. Adv. 6 (2020) eaba4098.
[13] H. Liu, Q. Liu, Y. Wang, et al., Chin. Chem. Lett. 33 (2022) 683–692.
[14] H. Li, L. Ma, C. Han, et al., Nano Energy 62 (2019) 550–587.
[15] Y. Niu, D. Wang, Y. Ma, et al., Chin. Chem. Lett. 33 (2022) 1430–1434.
[16] J. Abdulla, J. Cao, D. Zhang, et al., ACS Appl. Energy Mater. 4 (2021) 4602–4609.
[17] S. Higashi, S.W. Lee, J.S. Lee, et al., Nat. Commun. 7 (2016) 1–6.
[18] L. Ma, S. Chen, N. Li, et al., Adv. Mater. 32 (2020) 1908121.
[19] M. Zhou, S. Guo, G. Fang, et al., J. Energy Chem. 55 (2021) 549–556.
[20] V. Jabbari, T. Foroozan, R. Shahbazian-Yassar, et al., Adv. Energy Sustain. Res. 2 (2021) 2000082.
[21] J. Abdulla, J. Cao, P. Wangyao, et al., J. Met. Mater. Miner. 30 (2020) 1–8.
[22] Q. Zhang, L. Mei, X. Cao, et al., J. Mater. Chem. A 8 (2020) 15417–15444.
[23] T. Zhou, L. Zhu, L. Xie, et al., J. Colloid Interf. Sci. 605 (2022) 828–850.
[24] T. Zhou, L. Xie, Q. Han, et al., Chem. Eng. J. 445 (2022) 136789.
[25] T. Zhou, Q. Han, L. Xie, et al., Chem. Rec. 22 (2022) e202100275.
[26] Z. Yi, G. Chen, F. Hou, et al., Adv. Energy Mater. 11 (2021) 2003065.
[27] W. Zhang, H.L. Zhuang, L. Fan, et al., Sci. Adv. 4 (2018) eaar4410.
[28] S.-B. Wang, Q. Ran, R.Q. Yao, et al., Nat. Commun. 11 (2020) 1–9.
[29] Q. Yang, G. Liang, Y. Guo, et al., Adv. Mater. 31 (2019) 1903778.
[30] L. Ma, M.A. Schroeder, O. Borodin, et al., Nat. Energy 5 (2020) 743–749.
[31] J. Xie, Z. Liang, Y.C. Lu, Nat. Mater. 19 (2020) 1006–1011.
[32] L. Suo, O. Borodin, T. Gao, et al., Science 350 (2015) 938–943.
[33] L. Chen, J. Zhang, Q. Li, et al., ACS Energy Lett. 5 (2020) 968–974.
[34] P. Sun, L. Ma, W. Zhou, et al., Angew. Chem. Int. Ed. 133 (2021) 18395–18403.
[35] F. Wang, O. Borodin, T. Gao, et al., Nat. Mater. 17 (2018) 543–549.
[36] N. Dubouis, A. Serva, E. Salager, et al., J. Phys. Chem. Lett. 9 (2018) 6683–6688.
[37] J. Hao, X. Li, X. Zeng, et al., Energy Environ. Sci. 13 (2020) 3917–3949.
[38] D. Strmcnik, P.P. Lopes, B. Genorio, et al., Nano Energy 29 (2016) 29–36.
[39] X. Jia, C. Liu, Z.G. Neale, et al., Chem. Rev. 120 (2020) 7795–7866.
[40] D. Kundu, B.D. Adams, V. Duffort, et al., Nat. Energy 1 (2016) 1–8.
[41] H. Liang, Z. Cao, F. Ming, et al., Nano Lett. 19 (2019) 3199–3206.
[42] X. Wang, Z. Zhang, B. Xi, et al., ACS Nano 15 (2021) 9244–9272.
[43] H. Gan, J. Wu, R. Li, et al., Energy Storage Mater. 47 (2022) 602–610.
[44] X. Chen, W. Li, S. Hu, et al., Nano Energy 98 (2022) 107269.
[45] J. Zheng, Q. Zhao, T. Tang, et al., Science 366 (2019) 645–648.
[46] J. Cao, D. Zhang, C. Gu, et al., Adv. Energy Mater. 11 (2021) 2101299.
[47] H. Zhao, D. Lei, Y.B. He, et al., Adv. Energy Mater. 8 (2018) 1800266.
[48] X. Shi, G. Xu, S. Liang, et al., ACS Sustain. Chem. Eng. 7 (2019) 17737–17746.
[49] W. Guo, Z. Cong, Z. Guo, et al., Energy Storage Mater. 30 (2020) 104–112.
[50] Q. Jian, Z. Guo, L. Zhang, et al., Chem. Eng. J. 425 (2021) 130643.
[51] J. Cao, D. Zhang, X. Zhang, J. Mater. Chem. A 8 (2020) 9331–9344.
[52] J. Cao, D. Zhang, C. Gu, et al., Nano Energy 89 (2021) 106322.
[53] Q. Zhao, Y. Wang, W. Liu, et al., Adv. Mater. Interfaces 9 (2022) 2102254.
[54] G. Liang, J. Zhu, B. Yan, et al., Energy Environ. Sci. 15 (2022) 1086–1096.
[55] J. Zhou, L. Zhang, M. Peng, et al., Adv. Mater. 34 (2022) 2200131.
[56] P. Lin, J. Cong, J. Li, et al., Energy Storage Mater. 49 (2022) 172–180.
[57] Z. Lv, B. Wang, M. Ye, et al., ACS Appl. Mater. Interfaces 14 (2022) 1126–1137.
[58] J. Cao, D. Zhang, Y. Yue, et al., Chem. Eng. J. 426 (2021) 131893.
[59] A. Mauger, C.M. Julien, J.B. Goodenough, et al., J. Electrochem. Soc. 167 (2020) 070507.
[60] J.O. Besenhard, G. Eichinger, J. Electroanal. Chem. 68 (1976) 1.
[61] L. Yan, X. Zeng, Z. Li, et al., Mater. Today Energy 13 (2019) 323.
[62] M. Winter, B. Barnett, K. Xu, Chem. Rev. 118 (2018) 11433–11456.
[63] Z. Liu, Y. Huang, Y. Huang, et al., Chem. Soc. Rev. 49 (2020) 180–232.
[64] Y. Tian, Y. An, C. Wei, et al., Adv. Energy Mater. 11 (2021) 2002529.
[65] W. Yao, P. Zou, M. Wang, et al., Electrochem. Energy R. 4 (2021) 601–631.
[66] M.R. Palacin, Chem. Soc. Rev. 38 (2009) 2565–2575.
[67] F. Wu, J. Maier, Y. Yu, Chem. Soc. Rev. 49 (2020) 1569–1614.
[68] Z. Song, H. Zhou, Energy Environ. Sci. 6 (2013) 2280–2301.
[69] W. Li, K. Wang, S. Cheng, et al., Adv. Energy Mater. 9 (2019) 1900993.
[70] F. Wang, O. Borodin, T. Gao, et al., Nat. Mater. 17 (2018) 543.
[71] W.S.V. Lee, T. Xiong, X. Wang, et al., Small Methods 5 (2021) 2000815.
[72] D. Zhang, L. Li, Y. Zhang, J. Alloy. Compd. 869 (2021) 159352.
[73] L. Li, D. Zhang, Y. Gao, et al., J. Alloy. Compd. 862 (2021) 158551.
[74] Y. Yang, J. Xiao, J. Cai, et al., Adv. Funct. Mater. 31 (2021) 2005092.
[75] B. Zhao, S. Wang, Q. Yu, et al., J. Power Sources 504 (2021) 230076.
[76] J. Zhang, Q. Lei, Z. Ren, et al., ACS Nano 15 (2021) 17748–17756.
[77] Z. Lv, B. Wang, M. Ye, et al., ACS Appl. Mater. Interfaces 14 (2022) 1126–113.
[78] Q. Lei, J. Zhang, Z. Liang, et al., Adv. Energy Mater. 12 (2022) 2200547.
[79] Y. Du, B. Zhang, W. Zhou, et al., Energy Storage Mater. 51 (2022) 29–37.
[80] Y. Du, B. Zhang, R. Kang, et al., J. Mater. Chem. A 10 (2022) 16976–16985.
[81] P. Cai, K. Wang, J. Ning, et al., Adv. Energy Mater. 12 (2022) 2202182.
[82] Z. Liu, H. Su, Y. Yang, et al., Energy Storage Mater. 34 (2021) 211–228.
[83] C. Wu, J. Lou, J. Zhang, et al., Nano Energy 87 (2021) 106081.
[84] T. Xiong, Y. Zhang, Y. Wang, et al., J. Mater. Chem. A 8 (2020) 9006–9012.
[85] S. Wang, S. Lu, X. Yang, et al., J. Electroanal. Chem. 882 (2021) 115033.
[86] B. Wang, J. Yan, Y. Zhang, et al., Adv. Funct. Mater. 31 (2021) 2102827.
[87] X. Chen, R. Huang, M. Ding, et al., ACS Appl. Mater. Interfaces 14 (2022) 3961–3969.
[88] H. Peng, Q. Yu, S. Wang, et al., Adv. Sci. 6 (2019) 1900431.
[89] P. Poizot, J. Gaubicher, S. Renault, et al., Chem. Rev. 120 (2020) 6490–6557.
[90] Y. Chen, C. Wang, Acc. Chem. Res. 53 (2020) 2636–2647.
[91] Y. Wang, C. Wang, Z. Ni, et al., Adv. Mater. 32 (2020) 2000338.
[92] L. Yan, X. Zeng, Z. Li, et al., Mater. Today Energy 13 (2019) 323–330.
[93] N. Liu, X. Wu, Y. Zhang, et al., Adv. Sci. 7 (2020) 2000146.
[94] Y. Liu, M. Huang, F. Xiong, et al., Chem. Eng. J. 428 (2022) 131092.
[95] Z. Xu, M. Li, W. Sun, et al., Adv. Mater. 34 (2022) 2200077.
[96] M.S. Chae, S.T. Hong, Batteries 5 (2019) 3.
[97] Y. Liu, X. Zhou, X. Wang, et al., Chem. Eng. J. 420 (2021) 129629.
[98] X. Wang, Y. Wang, Y. Jiang, et al., Adv. Funct. Mater. 31 (2021) 2103210.
[99] Z. Chen, C. Li, Q. Yang, et al., Adv. Mater. 33 (2021) 2105426.
[100] Q. Zhang, T. Duan, M. Xiao, et al., ACS Appl. Mater. Interfaces 14 (2022) 25516–25523.
[101] D. Zhao, S. Chen, Y. Lai, et al., Nano Energy 100 (2022) 107520.
[102] Q. Zhao, Y. Zhu, S. Liu, et al., ACS Appl. Mater. Interfaces 14 (2022) 32066–32074.
[103] B. Long, Q. Zhang, T. Duan, et al., Adv. Sci. 9 (2022) 2204087.